Mon. Not. R. Astron. Soc. **387,** 871–882 (2008) doi:10.1111/j.1365-2966.2008.13284.x

Atomic data and electron-impact broadening effect in DO white dwarf atmospheres: Si VI

R. Hamdi,[1] N. Ben Nessib,[1] N. Milovanović,[2] L. Č. Popović,[2] M. S. Dimitrijević[2]★ and S. Sahal-Bréchot[3]

[1]*Groupe de Recherche en Physique Atomique et Astrophysique, Institut National des Sciences Appliquées et de Technologie, Centre Urbain Nord B. P. No. 676, 1080 Tunis Cedex, Tunisia*
[2]*Astronomical observatory, Volgina 7, 11160 Belgrade 74, Serbia*
[3]*Laboratoire d'Étude du Rayonnement et de la Matière en Astrophysique, UMR CNRS 8112, Observatoire de Paris-Meudon, 92195 Meudon, France*

Accepted 2008 April 3. Received 2008 March 28; in original form 2008 January 28

ABSTRACT

Energy levels, electric dipole transition probabilities and oscillator strengths in five times ionized silicon have been calculated in intermediate coupling. The present calculations were carried out with the general purpose atomic structure program SUPERSTRUCTURE. The relativistic corrections to the non-relativistic Hamiltonian are taken into account through the Breit–Pauli approximation. We have also introduced a semi-empirical correction [term energy corrections (TEC)] for the calculation of the energy levels. These atomic data are used to provide semiclassical electron-, proton- and ionized helium-impact linewidths and shifts for 15 Si VI multiplet. Calculated results have been used to consider the influence of Stark broadening for DO white dwarf atmospheric conditions.

Key words: atomic data – atomic processes – line: formation – stars: atmospheres – white dwarfs.

1 INTRODUCTION

Atomic data such as transition probabilities (*A*) play an important role in the diagnostics and modelling of laboratory plasmas (Griem 1974). Various kinetic processes appearing in plasma modelling need reliable knowledge of *A* values. Further, knowledge of *A* values gives a possibility for determination of coefficients (*B*) which characterize the absorption and stimulated emission. These processes are also important in laser physics. The classification of transitions and determination of energy levels are essential parts of the study of a laboratory spectrum. The lack of available atomic data limits our ability to infer reliably the properties of many cosmic plasmas and, hence, address many of the fundamental issues in astrophysics (Savin 2001).

Accurate Stark broadening parameters are important to obtain a reliable modelization of stellar interiors. The Stark broadening mechanism is also important for the investigation, analysis and modelling of *B*-type, and particularly *A*-type, stellar atmospheres, as well as for white dwarf atmospheres (see e.g. Popović et al. 2001; Dimitrijević et al. 2007).

Silicon, in various ionization stages, is detected in the atmospheres of DO white dwarfs (Werner, Dreizler & Wolff 1995). Si VI lines have been observed as well for example in coronal line regions of planetary nebulae NGC 6302 and 6537 (Casassus, Roche & Barlow 2000).

Uzelac and collaborators (Uzelac et al. 1993) studied plasma broadening of Ne II–Ne VI and F IV–F V experimentally and theoretically, they found that the results of simplified semiclassical (Griem 1974, equation 526) calculations show better agreement at higher ionization stages, while the modified semi-empirical formula (Dimitrijević & Konjević 1980) seems to be better for the low-ionization stages. Unfortunately, due to the lack of atomic data, most of the reported sophisticated semiclassical Stark broadening parameters relate to spectral lines of neutral- and low-ionization stages. In previous papers (Ben Nessib, Dimitrijević & Sahal-Bréchot 2004; Hamdi et al. 2007), we calculated Stark broadening parameters of quadruply ionized silicon and neon using SUPERSTRUCTURE and Bates & Damgaard (1949) method for oscillator strengths and we found that the difference is tolerable.

Si VI ion belongs to the fluorine-like sequence, its ground state configuration is $1s^2 2s^2 2p^5$ with the term $^2P^\circ$. In this work we present fine-structure energy levels, transition probabilities and oscillator strengths for Si VI ion. The atomic structure code SUPERSTRUCTURE was used, which allows for configuration interaction (CI), relativistic effects and semi-empirical term energy corrections (TEC). Calculated energies and oscillator strengths are used to provide Stark broadening parameters due to electron-, proton- and ionized helium impact of Si VI lines. The obtained Stark broadening parameters are used to investigate the influence of Stark broadening mechanism

★E-mail: mdimitrijevic@aob.bg.ac.yu

in hot, high gravity star atmospheres, as for example DO white dwarfs.

2 THE METHOD

In this work, the calculations were carried out with the general purpose atomic structure program SUPERSTRUCTURE (Eissner, Jones & Nussbaumer 1974), as modified by Nussbaumer & Storey (1978). The atomic model used to calculate energies of terms or levels and transition probabilities include 26 configurations: $2s^22p^5$, $2s2p^6$, $2s^22p^43\ell$, $2s^22p^44\ell$, $2s^22p^45\ell$, $2s^22p^46\ell$, $2s2p^53\ell$ and $2p^63\ell$ ($\ell \leqslant n - 1$). CI effects were fully taken into account. The wave functions are of the type

$$\Psi = \sum_i \Phi_i C_i, \tag{1}$$

where the basis functions Φ_i are constructed using one-electron orbitals. The latter are calculated with a scaled Thomas–Fermi statistical model potential or obtained from the Coulomb potential. For each radial orbital $P_{nl}(r)$, the potential can be adjusted using a parameter called λ. In the present case, those n- and l-dependent scaling parameters λ_{nl} were determined variationally by optimizing the weighted sum of the term energies. The P_{nl} are orthogonalized to each other such that the function P_{n_1l} is orthogonalized to the function P_{n_2l} when $n_2 < n_1$. The values adopted for the λ_{nl} parameters are presented in Table 1. In this approach the Hamiltonian is taken to be in the form

$$H = H_{\rm nr} + H_{\rm BP}, \tag{2}$$

relativistic corrections are included in Breit–Pauli Hamiltonian ($H_{\rm BP}$) as perturbation to the non-relativistic Hamiltonian ($H_{\rm nr}$). $H_{\rm BP}$ contains the one-electron operators for the mass correction, the Darwin contact term, the spin–orbit interaction in the field of the nucleus and the two-electron operators for spin–orbit, spin–other orbit and spin–spin interactions. We also use the so-called TEC introduced by Zeippen, Seaton & Morton (1977), in which the Hamiltonian matrix is empirically adjusted to give the best agreement between experimental energies and the final calculated term energies including the relativistic effects. In practice, the TEC for a given term is simply the difference between the calculated and measured energy of the lowest level in the multiplet.

Stark broadening parameter calculations have been performed within the semiclassical perturbation method (Sahal-Bréchot 1969a,b). A detailed description of this formalism with all the innovations is given in Sahal-Bréchot (1969a,b, 1974, 1991), Fleurier, Sahal-Bréchot & Chapelle (1977), Dimitrijević, Sahal-Bréchot & Bommier (1991) and Dimitrijević & Sahal-Bréchot (1996). The full half-width (w) and shift (d) of an electron-impact broadened spectral line can be expressed as

$$W = N \int v f(v)\,{\rm d}v \left[\sum_{i' \neq i} \sigma_{ii'}(v) + \sum_{f' \neq f} \sigma_{ff'}(v) + \sigma_{\rm el}\right] + W_{\rm R},$$
$$d = N \int v f(v)\,{\rm d}v \int_{R_3}^{R_{\rm D}} 2\pi\rho\,{\rm d}\rho \sin(2\varphi_{\rm p}), \tag{3}$$

where N is the electron density, $f(\upsilon)$ the Maxwellian velocity distribution function for electrons, ρ denotes the impact parameter of the incoming electron, i and f denote the initial and the final atomic energy levels and i' and f' their corresponding perturbing levels, while $W_{\rm R}$ gives the contribution of the Feshbach resonances (Fleurier et al. 1977). The inelastic cross-section $\sigma_{ii'}(\upsilon)$ can be expressed by an integral over the impact parameter of the transition probability $P_{jj'}(\rho, \upsilon)$ as

$$\sum_{j \neq j'} \sigma_{ii'}(\upsilon) = \frac{1}{2}\pi R_1^2 + \int_{R_1}^{R_{\rm D}} 2\pi\rho\,{\rm d}\rho \sum_{j \neq j'} P_{jj'}(\rho, \upsilon),\ j = i, f, \tag{4}$$

and the elastic cross-section is given by

$$\sigma_{\rm el} = 2\pi R_2^2 + \int_{R_2}^{R_{\rm D}} 2\pi\rho\,{\rm d}\rho \sin^2\delta,$$
$$\delta = \left(\varphi_{\rm p}^2 + \varphi_{\rm q}^2\right)^{1/2}. \tag{5}$$

The phase shifts $\varphi_{\rm p}$ and $\varphi_{\rm q}$ due, respectively, to the polarization potential (r^{-4}) and to the quadrupolar potential (r^{-3}) are given in section 3 of chapter 2 in Sahal-Bréchot (1969a), and $R_{\rm D}$ is the Debye radius. All the cut-offs R_1, R_2, R_3 are described in section 1 of chapter 3 in Sahal-Bréchot (1969b).

For electrons, hyperbolic paths due to the attractive Coulomb force were used, while for perturbing ions the hyperbolic paths are different since the force is repulsive. The formulae for the ion-impact widths and shifts are analogous to equations (3)–(5), without the resonance contribution to the width.

Table 1. Optimized parameters λ_{nl} adopted for the 26-configuration model calculation. Positive values for Thomas–Fermi–Dirac potential and negative values for Coulomb potential.

n, l	λ_{nl}	n, l	λ_{nl}	n, l	λ_{nl}	n, l	λ_{nl}
1s	1.4653	4s	1.1091	5d	1.1015	6f	−0.6629
2s	1.1844	4p	1.0960	5f	1.1135	6g	−1.0777
2p	1.1389	4d	1.1103	5g	1.0776	6h	−1.3002
3s	1.1078	4f	1.0478	6s	4.8162		
3p	1.0762	5s	1.1580	6p	6.2669		
3d	1.1808	5p	1.0902	6d	5.3865		

3 RESULTS AND DISCUSSION

The calculated *ab initio* energies for Si VI are listed in Table 2 along with experimentally determined energies for a number of levels taken from a National Institute of Standards and Technology (NIST) compilation. The configurations for which we present results are $2s^22p^5$, $2s2p^6$, $2s^22p^43\ell$, $2s^22p^44\ell'$; ℓ = s, p, d and ℓ' = s, p, d. We use the LS coupling scheme to designate excited energy.

Two different models are used for the determination of energy levels, the first contains the nine configurations of the model given in Section 2 and the second contains the totality of the 26 configurations. Both nine-configuration model and more elaborated 26-configuration one give energy levels in good agreement with the NIST values, indeed, our energies are lower than the NIST ones by less than 1 per cent except for the two first excited levels, i.e. $2p^5\ {}^2P^\circ_{1/2}$ and $2s2p^6\ {}^2S_{1/2}$. However, the results obtained by the second model are always more accurate that proves the importance of the CI. Besides, if a term is simply shifted relatively to the ground state, then the difference with observed energy should be essentially constant. In some terms the levels are not always in correct order. For example, the observed order of the levels of $2p^4(^3P)3d^4F$ is (9/2, 7/2, 5/2, 3/2) and the present order is (9/2, 3/2, 5/2, 7/2).

We use the calculated energies and the wavefunctions to calculate oscillator strengths and transition probabilities. With the aim of improving the quality of our wavefunctions, the $2s2p^6\ {}^2S_{1/2}$ level is corrected using TEC procedure (see Section 2). This method cannot

Table 2. Energy levels for Si VI in cm^{-1}. Key: a number assigned to each level; LS: LS term and parity (superscript ° designate an odd level); *J*: *J* value of the level; E_{9-conf}: *ab initio* energy levels, calculated with nine-configuration model; $E_{26-conf}$: *ab initio* energy levels, calculated with 26-configuration model; E_{NIST}: NIST values.

Key	Configuration	LS	*J*	E_{9-conf}	$E_{26-conf}$	E_{NIST}
1	$2p^5$	$^2P^\circ$	3/2	0	0	0
2			1/2	2 796	2 839	5 090
3	$2s2p^6$	^2S	1/2	435 632	426 462	406 497
4	$2p^4(^3P)3s$	^4P	5/2	971 851	982 366	990 516
5			1/2	975 520	986 496	995 470
6			3/2	975 969	987 021	993 640
7	$2p^4(^3P)3s$	^2P	3/2	987 370	999 127	1 005 430
8			1/2	987 692	999 494	1 009 118
9	$2p^4(^1D)3s$	^2D	5/2	1 024 374	1 036 129	1 041 416
10			3/2	1 024 884	1 036 533	1 041 472
11	$2p^4(^3P)3p$	$^4P^\circ$	3/2	1 052 168	1 061 210	1 069 854
12			5/2	1 052 404	1 061 401	1 068 813
13			1/2	1 053 583	1 062 874	1 071 129
14	$2p^4(^3P)3p$	$^4D^\circ$	7/2	1 059 089	1 070 621	1 078 935
15			1/2	1 061 265	1 073 242	1 083 003
16			3/2	1 062 447	1 074 609	1 082 215
17			5/2	1 062 788	1 074 942	1 080 700
18	$2p^4(^3P)3p$	$^2D^\circ$	5/2	1 068 139	1 080 203	1 086 796
19			3/2	1 068 477	1 080 547	1 089 547
20	$2p^4$ $(^3P)3p$	$^2P^\circ$	1/2	1 077 264	1 080 958	
21			3/2	1 075 947	1 084 287	1 092 171
22	$2p^4(^1S)3s$	^2S	1/2	1 071 075	1 084 295	1 094 449
23	$2p^4(^3P)3p$	$^4S^\circ$	3/2	1 074 673	1 087 671	1 093 752
24	$2p^4(^3P)3p$	$^2S^\circ$	1/2	1 094 162	1 088 558	
25	$2p^4(^1D)3p$	$^2F^\circ$	5/2	1 106 342	1 118 373	1 123 540
26			7/2	1 106 472	1 118 689	1 124 219
27	$2p^4(^1D)3p$	$^2D^\circ$	3/2	1 116 033	1 128 816	1 134 081
28			5/2	1 116 641	1 129 460	1 134 496
29	$2p^4(^1D)3p$	$^2P^\circ$	3/2	1 140 823	1 145 932	1 147 901
30			1/2	1 140 921	1 145 980	1 150 282
31	$2p^4(^1S)3p$	$^2P^\circ$	3/2	1 182 143	1 171 561	
32			1/2	1 182 942	1 172 417	
33	$2p^4(^3P)3d$	^4D	7/2	1 161 013	1 172 209	1 181 167
34			5/2	1 162 025	1 173 271	1 181 649
35			3/2	1 162 165	1 173 376	1 182 311
36			1/2	1 162 754	1 173 979	1 182 894
37	$2p^4(^3P)3d$	^4F	9/2	1 169 569	1 182 612	1 189 844
38			3/2	1 171 689	1 184 525	1 194 327
39			5/2	1 172 030	1 184 838	1 193 223
40			7/2	1 172 047	1 184 946	1 191 541
41	$2p^4(^3P)3d$	^4P	1/2	1 176 385	1 188 594	1 194 899
42			3/2	1 177 207	1 189 543	1 195 984
43			5/2	1 178 908	1 191 510	1 197 727
44	$2p^4(^3P)3d$	^2F	7/2	1 177 148	1 189 950	1 194 987
45			5/2	1 178 364	1 190 848	1 197 151
46	$2p^4(^3P)3d$	^2P	1/2	1 182 736	1 194 144	1 200 710
47			3/2	1 185 454	1 196 939	1 204 740
48	$2p^4(^3P)3d$	^2D	3/2	1 185 167	1 195 061	1 201 100
49			5/2	1 185 973	1 196 247	1 202 960
50	$2p^4(^1D)3d$	^2G	7/2	1 214 568	1 227 449	
51			9/2	1 214 715	1 227 538	1 232 671
52	$2p^4(^1D)3d$	^2S	1/2	1 223 636	1 234 097	1 239 190
53	$2p^4(^1$ $D)3d$	^2P	3/2	1 224 780	1 234 806	1 241 050
54			1/2	1 225 778	1 235 883	1 242 390
55	$2p^4(^1D)3d$	^2F	7/2	1 223 872	1 236 910	1 242 649
56			5/2	1 223 946	1 236 950	1 242 186
57	$2p^4(^1D)3d$	^2D	5/2	1 226 710	1 237 621	1 243 020
58			3/2	1 227 611	1 238 313	1 243 860
59	$2p^4(^1S)3d$	^2D	3/2	1 290 487	1 280 925	1 291 790
60			5/2	1 291 154	1 281 640	1 291 510
61	$2p^4(^3P)4s$	^4P	5/2	1 302 866	1 314 745	
62			1/2	1 305 283	1 317 544	
63			3/2	1 306 890	1 319 305	
64	$2p^4(^3P)4s$	^2P	3/2	1 308 844	1 321 429	1 329 900
65			1/2	1 310 323	1 323 045	
66	$2p^4(^3P)4p$	$^4P^\circ$	5/2	1 333 771	1 340 871	
67			3/2	1 333 474	1 340 979	
68			1/2	1 334 815	1 342 729	
69	$2p^4(^3P)4p$	$^4D^\circ$	7/2	1 335 203	1 347 589	
70			1/2	1 337 989	1 350 092	
71			3/2	1 338 555	1 351 294	
72			5/2	1 338 545	1 352 144	
73	$2p^4(^3P)4p$	$^2D^\circ$	5/2	1 339 973	1 351 228	
74			3/2	1 339 638	1 352 195	
75	$2p^4(^3P)4p$	$^2S^\circ$	1/2	1 340 521	1 352 722	
76	$2p^4(^3P)4p$	$^4S^\circ$	3/2	1 342 995	1 355 616	
77	$2p^4(^3P)4p$	$^2P^\circ$	3/2	1 349 411	1 359 114	
78			1/2	1 349 310	1 359 465	
79	$2p^4(^1D)4s$	^2D	5/2	1 352 262	1 365 126	1 371 820
80			3/2	1 352 767	1 365 515	
81	$2p^4(^3P)4d$	^4D	7/2	1 371 226	1 382 797	
82			5/2	1 372 174	1 384 161	
83			3/2	1 372 430	1 384 614	
84			1/2	1 373 107	1 385 519	
85	$2p^4(^3P)4d$	^4F	9/2	1 374 444	1 387 108	
86			7/2	1 376 125	1 388 760	
87			5/2	1 376 654	1 389 343	
88			3/2	1 376 461	1 389 348	
89	$2p^4(^3P)4d$	^4P	1/2	1 377 931	1 390 631	
90			3/2	1 379 041	1 391 893	
91			5/2	1 380 830	1 393 884	
92	$2p^4(^3P)4d$	^2F	5/2	1 380 128	1 392 885	
93			7/2	1 380 477	1 393 669	
94	$2p^4(^3P)4d$	^2P	1/2	1 381 851	1 393 521	1 402 490
95			3/2	1 384 583	1 396 287	1 403 050
96	$2p^4(^3P)4d$	^2D	3/2	1 385 040	1 395 603	
97			5/2	1 385 544	1 396 797	1 404 870
98	$2p^4(^3P)4p$	$^2F^\circ$	7/2	1 382 852	1 395 696	
99			5/2	1 382 929	1 395 739	
100	$2p^4(^1D)4p$	$^2D^\circ$	3/2	1 386 127	1 399 126	
101			5/2	1 386 673	1 399 653	
102	$2p^4(^1D)4p$	$^2P^\circ$	1/2	1 392 385	1 405 752	
103			3/2	1 392 362	1 405 797	
104	$2p^4(^1D)4s$	^2S	1/2	1 419 675	1 432 175	
105	$2p^4(^1D)4d$	^2G	7/2	1 421 515	1 434 310	
106			9/2	1 421 617	1 434 434	
107	$2p^4(^1D)4d$	^2P	3/2	1 424 977	1 436 510	
108			1/2	1 425 973	1 437 711	
109	$2p^4(^1D)4d$	^2F	7/2	1 424 368	1 437 280	
110			5/2	1 424 453	1 437 401	
111	$2p^4(^1D)4d$	^2D	5/2	1 425 961	1 438 109	1 444 340
112			3/2	1 426 992	1 438 858	1 445 010
113	$2p^4(^1D)4d$	^2S	1/2	1 427 833	1 440 235	
114	$2p^4(^1S)4p$	$^2P^\circ$	1/2	1 453 543	1 466 060	
115			3/2	1 453 658	1 466 257	
116	$2p^4(^1S)4d$	^2D	3/2	1 493 396	1 506 902	
117			5/2	1 494 092	1 507 702	

be applied for $2p^5\ ^2P^\circ_{1/2}$ level. Electric dipole transition probabilities and weighted oscillator strengths are presented in Table 3 for transition with lower level from one to 10 and upper level from three to 95. The majority of wavelengths are in extreme ultraviolet (XUV) region. F-like ions are of fundamental importance for current

Table 3. Transition probabilities (A_{ki}), calculated wavelengths (λ) and weighted oscillator strengths (gf) for Si VI spectrum. Present: this work; FF: Froese Fischer & Tachiev (2004); CT: Coutinho & Trigueiros (1999). The numbers in brackets denote powers of 10.

Transition	λ (Å)	$A_{ki}(s^{-1})$			gf			
		present	FF	NIST	present	FF	NIST	CT
1–3	246.004	1.805(10)	1.777(10)	1.77(10)	3.275(−01)	3.210(−01)	3.206(−01)	4.04(−01)
2–3	247.734	8.840(09)	8.517(09)	8.46(09)	1.627(−01)	1.576(−01)	1.573(−01)	2.00(−01)
1–4	101.795	8.982(07)	7.405(07)	7.51(07)	8.372(−04)	6.784(−04)	6.886(−04)	8.00(−04)
1–5	101.369	1.340(09)	8.423(06)	8.55(06)	4.128(−03)	2.547(−05)	2.588(−05)	
2–5	101.661	2.010(09)	2.624(08)	2.64(08)	6.229(−03)	8.016(−04)	8.072(−04)	9.00(−04)
1–6	101.315	1.019(08)	1.167(09)	1.18(09)	6.270(−04)	7.088(−03)	7.161(−03)	7.50(−03)
2–6	101.607	9.716(06)	1.010(08)	1.08(08)	6.016(−05)	6.194(−04)	6.266(−04)	6.00(−04)
1–7	100.087	6.667(10)	6.753(10)	6.74(10)	4.005(−01)	4.004(−01)	3.999(−01)	4.88(−01)
2–7	100.373	1.292(10)	1.098(10)	1.09(10)	7.803(−02)	6.574(−02)	6.561(−02)	7.90(−02)
1–8	100.051	2.509(10)	2.823(10)	2.82(10)	7.530(−02)	8.304(−02)	8.317(−02)	1.02(−01)
2–8	100.336	4.987(10)	5.156(10)	5.15(10)	1.505(−01)	1.532(−01)	1.531(−01)	1.86(−01)
1–9	96.513	3.189(10)	3.087(10)	3.08(10)	2.672(−01)	2.556(−01)	2.558(−01)	
1–10	96.475	4.625(09)	3.056(09)	3.03(09)	2.582(−02)	1.687(−02)	1.674(−02)	2.03(−02)
2–10	96.740	2.674(10)	2.796(10)	2.79(10)	1.501(−01)	1.558(−01)	1.559(−01)	1.94(−01)
3–11	152.739	1.064(05)	7.895(05)		1.488(−06)	1.077(−05)		
4–11	1268.336	3.944(08)	4.159(08)	4.11(08)	3.805(−01)	3.935(−01)	3.908(−01)	
5–11	1338.445	1.569(08)	1.624(08)	1.62(08)	1.685(−01)	1.746(−01)	1.749(−01)	1.89(−01)
6–11	1347.907	8.664(07)	9.855(07)	9.73(07)	9.440(−02)	1.010(−01)	1.004(−01)	1.07(−01)
7–11	1610.745	4.125(05)	5.789(04)	5.56(04)	6.418(−04)	8.312(−05)	8.035(−05)	
8–11	1620.320	1.353(07)	3.677(03)	3.79(03)	2.130(−02)	5.938(−06)	6.165(−06)	
9–11	3987.165	6.968(04)	1.627(04)	1.62(04)	6.643(−04)	1.218(−04)	1.199(−04)	
10–11	4052.352	7.466(03)	5.228(03)	5.44(03)	7.353(−05)	3.929(−05)	4.036(−05)	
4–12	1265.271	5.940(08)	5.712(08)	5.64(08)	8.554(−01)	8.322(−01)	8.279(−01)	8.72(−01)
6–12	1344.446	9.628(07)	1.104(08)	1.10(08)	1.565(−01)	1.744(−01)	1.753(−01)	1.91(−01)
7–12	1605.805	1.630(06)	2.988(05)	3.09(05)	3.781(−03)	6.648(−04)	6.918(−04)	
9–12	246.004	1.458(05)	2.110(03)	2.37(03)	2.054(−03)	2.554(−05)	2.837(−05)	
10–12	247.734	3.719(01)	2.179(02)	2.40(02)	5.410(−07)	2.646(−06)	2.890(−06)	
3–13	101.795	2.939(05)	4.160(05)		2.046(−06)	2.628(−06)		
5–13	1309.272	3.686(07)	7.502(07)	7.46(07)	1.894(−02)	3.900(−02)	3.899(−02)	
6–13	1318.325	5.969(08)	5.915(08)	5.85(08)	3.111(−01)	2.933(−01)	2.917(−01)	3.10(−01)
7–13	1568.682	1.079(06)	8.921(05)	9.49(05)	7.964(−04)	6.160(−04)	6.606(−04)	
8–13	1577.761	1.707(06)	4.217(05)	4.38(05)	1.274(−03)	3.268(−04)	3.419(−04)	
10–13	3796.252	1.573(04)	1.490(04)	1.49(04)	6.798(−05)	5.128(−05)	5.018(−05)	
4–14	1133.080	1.056(09)	1.033(09)	1.03(09)	1.626(+00)	1.581(+00)	1.577(+00)	1.71(+00)
9–14	2899.222	6.193(03)	3.205(03)	3.54(03)	6.244(−05)	2.776(−05)	3.019(−05)	
3–15	149.982	5.880(04)	1.367(06)	1.40(06)	3.966(−07)	8.972(−06)	9.141(−06)	9.00(−05)
5–15	1152.795	9.112(08)	8.776(08)	8.74(08)	3.631(−01)	3.426(−01)	3.419(−01)	3.70(−01)
6–15	1159.808	6.171(07)	1.290(08)	1.29(08)	2.489(−02)	4.836(−02)	4.841(−02)	
7–15	1349.252	9.550(05)	2.566(05)	2.58(05)	5.213(−04)	1.278(−04)	1.228(−04)	
8–15	1355.964	1.964(07)	7.280(05)	7.09(05)	1.083(−02)	3.998(−04)	3.899(−04)	
10–15	2724.120	6.668(04)	8.238(03)		1.484(−04)	1.454(−05)		
3–16	149.675	3.954(05)	5.543(05)	5.73(05)	5.312(−06)	7.292(−06)	7.516(−06)	
4–16	1084.091	2.953(07)	2.000(07)	2.03(07)	2.081(−02)	1.423(−02)	1.452(−02)	
5–16	1134.903	4.668(08)	4.842(08)	4.82(08)	3.606(−01)	3.850(−01)	3.837(−01)	4.13(−01)
6–16	1141.699	5.093(08)	4.957(08)	4.95(08)	3.981(−01)	3.781(−01)	3.768(−01)	4.11(−01)
7–16	1324.806	1.466(06)	1.213(03)	1.88(03)	1.543(−03)	1.232(−06)	1.909(−06)	
8–16	1331.276	2.832(07)	4.541(06)	4.53(06)	3.010(−02)	5.094(−03)	5.081(−03)	
9–16	2598.741	7.183(04)	8.858(03)	9.91(03)	2.909(−04)	3.241(−05)	3.572(−05)	
10–16	2626.277	1.035(02)	1.337(04)	1.45(04)	4.281(−07)	4.908(−05)	5.236(−05)	
4–17	1080.192	2.103(08)	1.903(08)	1.91(08)	2.207(−01)	2.100(−01)	2.113(−01)	2.38(−01)
6–17	1137.375	8.616(08)	7.873(08)	7.83(08)	1.003(+00)	9.320(−01)	9.289(−01)	9.98(−01)
7–17	1318.987	7.133(06)	1.864(07)	1.86(07)	1.116(−02)	2.957(−02)	2.958(−02)	
9–17	2576.446	2.564(03)	8.978(03)	9.31(03)	1.531(−05)	5.316(−05)	5.432(−05)	
4–18	1022.110	5.562(05)	1.307(07)	1.33(07)	5.227(−04)	1.265(−02)	1.285(−02)	
6–18	1073.164	1.749(07)	2.238(07)	2.22(07)	1.811(−02)	2.313(−02)	2.301(−02)	
7–18	1233.405	8.506(08)	8.032(08)	8.02(08)	1.164(+00)	1.090(−01)	1.088(+00)	
9–18	2268.921	7.863(04)	2.465(05)	2.49(05)	3.641(−04)	1.090(−03)	1.086(−03)	
10–18	2289.882	1.355(02)	6.522(03)	6.85(03)	6.391(−07)	2.892(−05)	2.999(−05)	
3–19	148.357	2.047(06)	1.279(07)		2.702(−05)	1.645(−04)		
4–19	1018.526	8.703(06)	2.181(06)	2.75(06)	5.415(−03)	1.326(−03)	1.336(−03)	
5–19	1063.250	9.488(07)	2.892(06)		6.433(−02)	1.952(−03)	1.862(−03)	
6–19	1063.250	1.100(05)	1.283(06)	1.22(06)	7.545(−05)	8.336(−04)	7.961(−04)	

Table 3 – *continued*

Transition	λ (Å)	$A_{ki}(s^{-1})$ present	FF	NIST	gf present	FF	NIST	CT
7–19	1228.189	9.754(07)	4.377(08)	4.54(08)	8.824(−02)	3.701(−01)	3.845(−01)	3.66(−01)
8–19	1233.748	6.973(08)	3.698(08)	3.48(08)	6.365(−01)	3.420(−01)	3.221(−01)	
9–19	2251.333	3.457(05)	6.305(06)	7.30(06)	1.051(−03)	1.648(−02)	1.887(−02)	
10–19	2271.969	4.466(04)	2.421(06)	2.63(06)	1.382(−04)	6.344(−03)	6.807(−03)	
3–20	148.267	1.378(08)	8.949(07)		9.085(−04)	5.760(−04)		
5–20	1058.626	6.333(05)	1.717(05)		2.128(−04)	5.804(−05)		
6–20	1064.537	6.918(06)	1.331(06)		2.351(−03)	4.332(−04)		
7–20	1222.023	5.861(08)	6.643(08)		2.624(−01)	2.813(−01)		
8–20	1227.526	6.666(07)	5.304(07)		3.012(−02)	2.458(−02)		
10–20	2250.959	2.878(07)	2.829(07)		4.373(−02)	3.719(−02)		
3–21	147.538	1.880(08)	1.114(08)	1.10(08)	2.454(−03)	1.422(−03)	1.339(−03)	
4–21	981.153	1.120(07)	7.761(06)	5.01(06)	6.464(−03)	4.476(−03)	2.904(−03)	
5–21	1022.589	4.986(06)	1.343(07)	1.08(07)	3.127(−03)	8.554(−03)	6.902(−03)	
6–21	1028.103	1.619(07)	2.197(06)		1.026(−02)	1.348(−03)		
7–21	1174.254	5.806(08)	2.535(08)	2.33(08)	4.801(−01)	2.008(−01)	1.853(−01)	2.24(−01)
8–21	1179.334	4.876(07)	4.094(08)	4.31(08)	4.067(−02)	3.538(−01)	3.741(−01)	3.42(−01)
9–21	2076.504	4.517(07)	4.361(07)	4.31(07)	1.168(−01)	1.018(−01)	1.002(−01)	
10–21	2094.047	5.294(06)	3.415(06)	3.31(06)	1.392(−02)	7.996(−03)	7.726(−03)	
1–22	92.226	2.083(10)	1.964(10)	1.96(10)	5.314(−02)	4.908(−02)	4.920(−02)	6.70(−02)
2–22	92.468	1.110(10)	1.232(10)	1.23(10)	2.845(−02)	3.108(−02)	3.097(−02)	4.26(−02)
3–23	146.805	5.237(06)	1.548(05)		6.769(−05)	1.968(−06)		
4–23	949.626	7.718(08)	6.774(08)	6.81(08)	4.174(−01)	3.808(−01)	3.837(−01)	3.48(−01)
5–23	988.389	3.575(08)	3.063(08)	3.08(08)	2.095(−01)	1.899(−01)	1.909(−01)	1.89(−01)
6–23	993.539	5.751(08)	5.521(08)	5.52(08)	3.405(−01)	3.301(−01)	3.303(−01)	3.30(−01)
7–23	1129.379	4.435(06)	4.529(05)	5.45(04)	3.393(−03)	3.484(−04)	4.197(−05)	
8–23	1134.078	3.772(06)	7.482(06)	5.32(06)	2.909(−03)	6.270(−03)	4.456(−03)	
9–23	1940.178	1.976(06)	1.302(06)		4.461(−03)	2.892(−03)		
10–23	1955.485	2.723(04)	9.887(04)		6.245(−05)	2.200(−04)		
3–24	146.615	4.880(07)	2.590(07)		3.145(−04)	1.644(−04)		
5–24	979.803	4.553(07)	2.065(06)		1.311(−02)	6.328(−04)		
6–24	984.864	1.963(03)	3.411(06)		5.710(−07)	1.008(−03)		
7–24	1118.182	2.447(08)	1.833(08)		9.173(−02)	6.964(−02)		
8–24	1122.788	7.678(08)	6.707(08)		2.902(−01)	2.772(−01)		
10–24	1922.160	1.678(07)	2.055(07)		1.859(−02)	2.237(−02)		
5–25	735.260	4.657(06)			2.265(−03)			
6–25	761.314	5.428(05)	1.357(04)	1.51(04)	2.830(−04)	7.164(−06)	8.035(−06)	
7–25	838.603	7.411(04)	7.983(04)		4.688(−05)	5.100(−05)		
9–25	1215.905	8.749(07)	7.805(07)	7.65(07)	1.163(−01)	1.035(−01)	1.020(−01)	1.09(−01)
10–25	1221.899	7.763(08)	7.612(08)	7.56(08)	1.043(+00)	1.011(+00)	1.006(+00)	1.11(+00)
4–26	733.553	8.310(05)	1.120(05)	1.20(05)	5.363(−04)	7.446(−05)	8.035(−05)	
9–26	1211.242	8.876(08)	8.628(08)	8.56(08)	1.562(+00)	1.501(+00)	1.499(+00)	1.64(+00)
3–27	138.443	1.456(03)	4.078(06)	4.89(06)	1.674(−08)	4.622(−05)		
4–27	682.827	3.924(05)	6.054(04)	6.24(04)	1.097(−04)	1.749(−05)	1.811(−05)	
5–27	702.641	1.011(06)	5.116(-1)	1.89(00)	2.994(−04)	1.584(−10)	5.902(−10)	
6–27	705.240	1.533(06)	1.283(06)	4.40(05)	4.573(−04)	1.294(−04)	1.339(−04)	
7–27	771.072	1.238(06)	1.967(07)	2.00(07)	4.413(−04)	7.076(−03)	7.244(−03)	
8–27	773.259	5.680(06)	5.306(06)	5.19(06)	2.037(−03)	2.024(−03)	1.995(−03)	
9–27	1078.900	1.254(08)	7.247(07)	7.17(07)	8.756(−02)	5.049(−02)	5.023(−02)	
10–27	1083.616	1.118(09)	1.117(09)	1.11(09)	7.875(−01)	7.792(−01)	7.798(−01)	8.03(−01)
4–28	679.840	2.305(07)	4.734(05)	4.88(05)	9.584(−03)	2.040(−04)	2.118(−04)	
6–28	702.055	4.910(06)	5.481(03)	4.62(03)	2.177(−03)	2.467(−06)	2.094(−06)	
7–28	767.266	6.267(06)	1.070(07)	1.05(07)	3.319(−03)	5.740(−03)	5.675(−03)	
9–28	1071.462	1.150(09)	1.100(09)	1.10(09)	1.187(+00)	1.140(+00)	1.140(+00)	1.17(+00)
10–28	1076.114	1.288(08)	1.137(08)	1.13(08)	1.342(−01)	1.179(−01)	1.174(−01)	1.18(−01)
3–29	135.238	5.172(08)	7.112(08)	7.11(08)	5.673(−03)	7.758(−03)	7.762(−03)	
4–29	611.374	2.805(07)	5.525(05)	5.48(05)	6.287(−03)	1.326(−04)	1.327(−04)	
5–29	627.211	2.072(07)	1.148(05)	1.09(05)	4.888(−03)	2.936(−05)	2.818(−05)	
6–29	629.281	2.656(05)	1.930(07)	1.92(07)	6.306(−05)	4.820(−03)	4.841(−03)	
7–29	681.173	1.678(09)	1.402(09)	1.38(09)	4.670(−01)	4.104(−01)	4.083(−01)	4.32(−01)
8–29	682.880	3.009(08)	2.957(08)	2.92(08)	8.415(−02)	9.122(−02)	9.078(−02)	9.61(−02)
9–29	910.722	1.294(09)	1.235(09)	1.23(09)	6.436(−01)	6.498(−01)	6.486(−01)	
10–29	914.081	1.412(08)	5.801(07)	5.69(07)	7.075(−02)	3.054(−02)	3.013(−02)	
3–30	135.230	5.478(08)	8.058(08)	8.06(08)	3.004(−03)	4.368(−03)	4.355(−03)	

Table 3 – *continued*

Transition	λ (Å)	$A_{ki}(s^{-1})$			gf			
		present	FF	NIST	present	FF	NIST	CT
5–30	627.022	7.195(07)	3.778(06)	3.77(06)	8.482(−03)	4.686(−04)	4.720(−04)	
6–30	629.090	1.571(05)	4.630(06)	4.61(06)	1.864(−05)	5.608(−04)	5.636(−04)	
7–30	680.950	6.378(08)	4.582(08)	4.52(08)	8.868(−02)	6.496(−02)	6.411(−02)	6.83(−02)
8–30	682.655	1.200(09)	1.070(09)	1.06(09)	1.677(−01)	1.596(−01)	1.588(−01)	1.68(−01)
10–30	913.679	1.459(09)	1.448(09)	1.44(09)	3.653(−01)	3.649(−01)	3.647(−01)	3.73(−01)
3–31	130.708	8.779(08)	6.247(08)		8.995(−03)	6.224(−03)		
4–31	528.555	4.887(06)	1.410(05)		8.188(−04)	2.283(−05)		
5–31	540.350	3.953(06)	1.024(04)		6.922(−04)	1.745(−06)		
6–31	541.886	6.974(06)	2.069(06)		1.228(−03)	3.461(−04)		
7–31	579.929	2.418(08)	1.207(08)		4.877(−02)	2.297(−02)		
8–31	581.166	6.960(07)	2.686(07)		1.410(−02)	5.334(−03)		
9–31	738.377	1.559(05)	2.646(06)		5.098(−05)	7.962(−04)		
10–31	740.583	2.238(04)	1.572(06)		7.363(−06)	4.732(−04)		
3–32	130.562	8.400(08)	5.510(08)		4.293(−03)	2.744(−03)		
5–32	537.865	8.805(06)	6.903(05)		7.638(−04)	5.880(−05)		
6–32	539.386	1.317(03)	7.534(05)		1.149(−07)	6.296(−05)		
7–32	577.068	8.320(07)	7.216(07)		8.308(−03)	6.860(−03)		
8–32	578.292	1.931(08)	1.451(08)		1.937(−02)	1.438(−02)		
10–32	735.923	5.602(06)	1.894(06)		9.097(−04)	2.847(−04)		
1–34	85.232	8.382(06)	2.275(07)	2.30(07)	5.477(−05)	1.464(−04)	1.482(−04)	
1–35	85.224	9.086(05)	1.456(08)	1.45(08)	3.958(−06)	6.244(−04)	6.237(−04)	
2–35	85.431	6.482(07)	3.464(07)	3.50(07)	2.837(−04)	1.498(−04)	1.517(−04)	
1–36	85.181	8.300(07)	8.691(07)	8.61(07)	1.806(−04)	1.861(−04)	1.845(−04)	
2–36	85.387	1.621(08)	2.003(08)	1.99(08)	3.545(−04)	4.328(−04)	4.295(−04)	
1–38	84.422	8.666(07)	1.172(09)	1.18(09)	3.704(−04)	4.921(−03)	4.954(−03)	1.03(−01)
2–38	84.625	4.078(08)	2.408(09)	2.44(09)	1.751(−03)	1.020(−02)	1.035(−02)	1.96(−02)
1–41	84.133	8.295(08)	1.409(09)		1.761(−03)	2.958(−03)		
2–41	84.334	5.368(08)	1.743(07)		1.145(−03)	3.690(−05)		
1–42	84.066	4.006(08)	2.740(09)		1.698(−03)	1.148(−02)		
2–42	84.267	3.639(07)	5.164(08)		1.550(−04)	2.182(−03)		3.00(−04)
1–43	83.927	1.359(08)	3.789(08)		8.612(−04)	2.374(−03)		1.46(−02)
1–45	83.974	1.817(10)	2.211(10)		1.153(−01)	1.386(−01)		
1–46	83.742	3.143(10)	2.980(10)	2.99(10)	6.608(−02)	6.196(−02)	6.194(−02)	5.95(−02)
2–46	83.942	5.476(10)	4.368(10)	4.36(10)	1.157(−01)	9.156(−02)	9.141(−02)	8.40(−02)
1–47	83.546	6.063(10)	1.686(10)	1.77(10)	2.538(−01)	6.960(−02)	7.227(-02)	3.09(−01)
2–47	83.745	2.522(10)	9.938(10)	9.74(10)	1.061(−01)	4.138(−01)	4.064(−01)	4.00(−04)
1–48	83.678	4.790(10)	9.699(10)	9.60(10)	2.012(−01)	4.028(−01)	3.990(−01)	7.03(−02)
2–48	83.877	1.934(11)	9.296(10)	9.47(10)	8.162(−01)	3.894(−01)	3.981(−01)	8.26(−01)
1–49	83.595	2.281(11)	2.341(11)	2.34(11)	1.434(+00)	1.545(+00)	1.452(+00)	1.27(+00)
1–52	81.031	3.016(11)	2.850(11)	2.76(11)	5.939(−01)	5.556(−01)	5.395(−01)	6.00(−01)
2–52	81.218	7.742(10)	7.643(10)	8.45(10)	1.531(−01)	1.502(−01)	1.663(−01)	2.13(−01)
1–53	80.984	3.209(11)	2.749(11)	2.74(11)	1.262(+00)	1.068(+00)	1.069(+00)	1.33(+00)
2–53	81.171	3.233(10)	5.658(10)	5.67(10)	1.278(−01)	2.218(−01)	2.218(−01)	2.91(−01)
1–54	80.914	6.868(10)	6.732(10)	6.85(10)	1.348(−01)	1.306(−01)	1.333(−01)	2.11(−01)
2–54	81.100	2.860(11)	2.804(11)	2.78(11)	5.640(−01)	5.484(−01)	5.457(−01)	6.27(−01)
1–56	80.844	3.445(10)	6.766(10)		2.025(−01)	3.939(−01)		7.83(−02)
1–57	80.800	1.848(11)	1.335(11)	1.31(11)	1.085(+00)	7.764(−01)	7.603(−01)	1.59(+00)
1–58	80.755	1.352(10)	3.492(10)	3.50(10)	5.289(−02)	1.351(−01)	1.355(−01)	1.97(−01)
2–58	80.941	1.969(11)	1.891(11)	1.89(11)	7.735(−01)	7.380(−01)	7.362(−01)	1.01(+00)
1–59	78.069	8.919(09)	7.731(09)	7.74(09)	3.260(−02)	2.776(−02)	2.779(−02)	
2–59	78.242	4.642(10)	5.577(10)	5.57(10)	1.704(−01)	2.018(−01)	2.018(−01)	2.72(−01)
1–60	78.025	4.737(10)	5.054(10)	5.05(10)	2.594(−01)	2.723(−01)	2.722(−01)	3.75(−01)
1–61	76.060	2.957(07)			1.539(−04)			
1–62	75.899	3.236(09)			5.589(−03)			
2–62	76.063	6.405(09)			1.111(−02)			
1–63	75.797	1.243(09)			4.281(−03)			1.14(−02)
2–63	75.961	2.661(08)			9.209(−04)			
1–64	75.676	2.243(10)		1.24(10)	7.702(−02)		4.197(−02)	4.21(−02)
2–64	75.839	4.741(09)		2.11(09)	1.635(−02)		7.194(−03)	7.20(−03)
1–65	75.583	5.689(09)			9.746(−03)			
2–65	75.746	1.202(10)			2.069(−02)			
4–66	278.937	1.029(10)			7.204(−01)			
6–66	282.606	2.931(09)			2.106(−01)			

Table 3 – *continued*

Transition	λ (Å)	$A_{ki}(s^{-1})$ present	FF	NIST	gf present	FF	NIST	CT
7–66	292.617	2.511(07)			1.934(−03)			
9–66	328.147	5.179(07)			5.016(−03)			
10–66	328.582	6.473(03)			6.287(−07)			
3–67	107.011	3.996(06)			2.744(−05)			
4–67	278.853	6.399(09)			2.984(−01)			
5–67	282.101	3.730(09)			1.780(−01)			
6–67	282.519	1.629(09)			7.796(−02)			
7–67	292.524	1.005(07)			5.159(−04)			
8–67	292.839	4.215(08)			2.168(−02)			
9–67	328.031	2.309(07)			1.490(−03)			
10–67	328.466	2.775(06)			1.796(−04)			
3–68	106.811	3.368(06)			1.152(−05)			
5–68	280.715	1.075(09)			2.539(−02)			
6–68	281.129	1.059(10)			2.511(−01)			
7–68	291.034	3.005(07)			7.632(−04)			
8–68	291.345	6.976(07)			1.776(−03)			
10–68	326.587	8.116(06)			2.596(−04)			
4–69	273.806	3.264(09)			2.935(−01)			
9–69	321.069	7.827(06)			9.678(−04)			
3–70	105.978	6.730(03)			2.266(−08)			
5–70	275.031	3.121(09)			7.079(−02)			
6–70	275.428	3.863(02)			8.788(−09)			
7–70	284.929	8.093(04)			1.970(−06)			
8–70	285.227	1.165(08)			2.841(−03)			
10–70	318.919	1.142(04)			3.482(−07)			
3–71	105.843	1.511(06)			1.011(−05)			
4–71	271.056	9.192(06)			4.050(−04)			
5–71	274.125	1.417(09)			6.385(−02)			
6–71	274.519	1.151(09)			5.201(−02)			
7–71	283.956	3.861(04)			1.867(−06)			
8–71	284.252	2.438(08)			1.181(−02)			
9–71	317.295	4.312(06)			2.603(−04)			
10–71	317.701	6.615(04)			4.004(−06)			
4–72	270.433	5.068(07)			3.334(−03)			
6–72	273.880	1.299(09)			8.765(−02)			
7–72	283.272	2.124(09)			1.533(−01)			
9–72	316.441	3.720(04)			3.351(−06)			
10–72	316.845	3.494(05)			3.155(−05)			
4–73	271.104	2.072(08)			1.370(−02)			
6–73	274.569	1.876(09)			1.272(−01)			
7–73	284.009	8.893(08)			6.453(−02)			
9–73	317.361	2.303(06)			2.086(−04)			
10–73	317.768	6.699(06)			6.085(−04)			
3–74	105.742	2.059(05)			1.381(−06)			
4–74	270.396	1.558(08)			6.832(−03)			
5–74	273.449	5.931(08)			2.660(−02)			
6–74	273.842	6.104(05)			2.745(−05)			
7–74	283.232	3.949(08)			1.900(−02)			
8–74	283.526	2.129(09)			1.026(−01)			
9–74	316.390	1.947(06)			1.169(−04)			
10–74	316.795	1.613(06)			9.709(−05)			
3–75	105.683	1.462(07)			4.896(−05)			
5–75	273.056	1.449(06)			3.239(−05)			
6–75	273.447	1.060(07)			2.376(−04)			
7–75	282.809	2.598(09)			6.230(−02)			
8–75	283.103	5.264(07)			1.265(−03)			
10–75	316.266	4.386(08)			1.315(−02)			
3–76	105.361	2.021(06)			1.345(−05)			
4–76	267.917	3.085(08)			1.328(−02)			
5–76	270.915	1.073(09)			4.722(−02)			
6–76	271.300	1.127(09)			4.973(−02)			
7–76	280.513	1.603(07)			7.565(−04)			
8–76	280.802	3.923(07)			1.855(−03)			

Table 3 – *continued*

Transition	λ (Å)	$A_{ki}(s^{-1})$ present	FF	NIST	gf present	FF	NIST	CT
9–76	313.002	1.264(06)			7.425(−05)			
10–76	313.398	1.091(06)			6.425(−05)			
3–77	104.974	4.741(07)			3.133(−04)			
4–77	265.429	3.542(06)			1.497(−04)			
5–77	268.371	6.593(07)			2.848(−03)			
6–77	268.750	7.602(06)			3.293(−04)			
7–77	277.787	1.359(09)			6.288(−02)			
8–77	278.07	1.709(08)			7.925(−03)			
9–77	309.612	1.217(09)			6.997(−02)			
10–77	309.999	1.274(08)			7.344(−03)			
3–78	104.935	3.845(07)			1.270(−04)			
5–78	268.119	1.251(08)			2.696(−03)			
6–78	268.497	1.917(07)			4.144(−04)			
7–78	277.517	1.251(06)			2.888(−05)			
8–78	277.800	1.619(09)			3.747(−02)			
10–78	309.663	8.910(08)			2.562(−02)			
1–79	73.253	9.110(09)		8.24(09)	4.398(−02)		3.935(−02)	3.94(−02)
1–80	73.232	1.305(09)			4.198(−03)			
2–80	73.385	7.299(09)			2.357(−02)			
1–82	72.246	2.920(08)			1.371(−03)			
1–83	72.222	1.216(02)			3.802(−10)			
2–83	72.371	2.423(08)			7.611(−04)			
1–84	72.175	5.005(08)			7.818(−04)			
2–84	72.323	9.647(08)			1.513(−03)			
1–87	71.976	2.262(10)			1.054(−01)			1.89(−01)
1–88	71.976	1.382(08)			4.293(−04)			
2–88	72.124	6.586(08)			2.055(−03)			1.03(−01)
1–89	71.910	2.267(09)			3.515(−03)			
2–89	72.057	3.055(09)			4.756(−03)			
1–90	71.845	1.208(09)			3.740(−03)			2.35(−02)
2–90	71.991	2.033(07)			6.318(−05)			2.00(−04)
1–91	71.742	1.462(09)			6.769(−03)			1.96(−02)
1–92	71.793	1.906(10)			8.839(−02)			
1–94	71.761	2.760(10)		2.19(10)	4.261(−02)		3.341(−02)	3.34(−02)
2–94	71.907	5.142(10)		3.56(10)	7.972(−02)		5.457(−02)	5.47(−02)
1–95	71.761	2.760(10)		7.20(10)	4.261(−02)			
2–95	71.907	5.142(10)		3.26(07)	7.972(−02)		1.000(−04)	1.00(−04)

X-ray laser research. Our transition probabilities are compared with NIST values and multiconfiguration Hartree–Fock (MCHF) results of Froese Fischer & Tachiev (2004), who use the observed energies for the calculation of transition probabilities. The agreement is by less than 30 per cent for 70 per cent of strong transitions ($A > 10^8$ s^{-1}) of NIST compilation. The agreement is much less for weak ones. For weighted oscillator strengths, comparison is made also with Coutinho & Trigueiros (1999) results obtained using multiconfiguration Hartree–Fock relativistic (HFR) approach. In their work the adjusted energy levels were used to optimize the electrostatic parameters, these optimized parameters were used again to calculate the gf values. In general, our oscillator strengths are in good agreement with the other works except for a few transitions as for example 2–5, 1–6, 2–6, 2–38 for which we observe large disagreement. For the transitions 1–47, 2–48, 2–42 our oscillator strengths agree better with Coutinho & Trigueiros results. On the other hand, for the transitions 2–47, 1–48, 1–56 the agreement with Froese-Fischer & Tachiev values is better. For the transitions 3–15, 1–38 all three methods give different results. The inclusion of a larger number of configurations has an important effect on wavefunctions and *A* values. TEC of the $2s2p^6\ ^2S_{1/2}$ level improve slightly our results. For example for the 2–3 transition our *A* value was 1.022E+10 s^{-1} and became 8.840E+09 s^{-1}, NIST one is 8.46E+09 s^{-1}. The correction of quartet terms do not improve the results.

By combining the SUPERSTRUCTURE code for calculating energy levels and oscillator strengths and the code for the Stark broadening calculations, we calculated Stark broadening parameters. Calculated Stark broadening widths [full width at half-maximum (FWHM)] and shifts for a perturber densities of 10^{17} cm^{-3} and temperatures from 50 000 up to 800 000 K are shown in Table 4 for electron-, proton- and singly ionized helium-impact broadening. Such temperatures are of interest for the modelling and analysis of X-ray spectra, such as the spectra obtained by *Chandra*, modelling of some hot star atmospheres (e.g. DO white dwarf and PG 1195), subphotospheric layers, soft X-ray lasers and laser produced plasmas. Higher temperatures are of interest for fusion plasma as well as for stellar interiors.

We also specify a parameter *C* (Dimitrijević & Sahal-Bréchot 1984), which gives an estimate for the maximal perturber density for which the line may be treated as isolated, when it is divided by the corresponding FWHM. For each value given in Table 4 the collision volume *V* multiplied by the perturber density *N* is much less than one and the impact approximation is valid (Sahal-Bréchot 1969a,b).

Table 4. This table gives electron-, proton- and singly charged helium-impact broadening parameters for Si VI lines calculated using SUPERSTRUCTURE oscillator strength, for a perturber density of 10^{17} cm^{-3} and temperature of 50 000 to 800 000 K. Transitions, averaged wavelength for the multiplet (in Å) and parameter C are also given. This parameter when divided with the corresponding Stark width gives an estimate for the maximal perturber density for which the line may be treated as isolated. w_e: electron-impact full Stark width at half-maximum; d_e: electron-impact Stark shift; $w_H{}^+$: proton-impact full Stark width at half-maximum; $d_H{}^+$: proton-impact Stark shift; $w_{He}{}^+$: singly charged helium-impact full Stark width at half-maximum; $d_{He}{}^+$: singly charged helium-impact Stark shift; w_{MSE}: electron-impact full Stark width at half-maximum calculated by Dimitrijević (1993) using modified semi-empirical formula (Dimitrijević & Konjević 1980).

Transition	T (K)	w_e	d_e	w_H^+	d_H^+	w_{He}^+	d_{He}^+	w_{MSE}
Si VI 3S-3P	50000	0.750E-02	−0.577E-04	0.360E-04	−0.260E-04	0.687E-04	−0.500E-04	0.415E-02
1226.7 Å	100000	0.532E-02	−0.739E-04	0.897E-04	−0.516E-04	0.173E-03	−0.103E-03	0.294E-02
$C = 0.11$E+21	200000	0.387E-02	−0.784E-04	0.177E-03	−0.920E-04	0.344E-03	−0.185E-03	0.212E-02
	400000	0.291E-02	−0.100E-03	0.269E-03	−0.139E-03	0.529E-03	−0.280E-03	0.169E-02
	800000	0.227E-02	−0.888E-04	0.347E-03	−0.189E-03	0.693E-03	−0.384E-03	0.147E-02
Si VI 3S-3P	50000	0.681E-02	−0.660E-04	0.346E-04	−0.294E-04	0.660E-04	−0.566E-04	0.375E-02
1187.2 Å	100000	0.486E-02	−0.841E-04	0.866E-04	−0.582E-04	0.167E-03	−0.116E-03	0.265E-02
$C = 0.67$E+20	200000	0.354E-02	−0.890E-04	0.171E-03	−0.102E-03	0.335E-03	−0.205E-03	0.191E-02
	400000	0.267E-02	−0.109E-03	0.262E-03	−0.150E-03	0.517E-03	−0.304E-03	0.152E-02
	800000	0.208E-02	−0.993E-04	0.340E-03	−0.203E-03	0.678E-03	−0.412E-03	0.132E-02
Si VI 3S′-3P′	50000	0.716E-02	−0.644E-04	0.471E-04	−0.212E-04	0.899E-04	−0.409E-04	0.389E-02
1228.8 Å	100000	0.509E-02	−0.599E-04	0.113E-03	−0.424E-04	0.219E-03	−0.842E-04	0.275E-02
$C = 0.72$E+20	200000	0.370E-02	−0.615E-04	0.213E-03	−0.771E-04	0.416E-03	−0.155E-03	0.198E-02
	400000	0.278E-02	−0.770E-04	0.314E-03	−0.119E-03	0.618E-03	−0.241E-03	0.158E-02
	800000	0.216E-02	−0.691E-04	0.389E-03	−0.164E-03	0.774E-03	−0.331E-03	0.137E-02
Si VI 3S′-3P′	50000	0.572E-02	−0.376E-04	0.399E-04	−0.131E-04	0.762E-04	−0.252E-04	0.312E-02
1087.4 Å	100000	0.408E-02	−0.358E-04	0.948E-04	−0.263E-04	0.183E-03	−0.521E-04	0.220E-02
$C = 0.56$E+20	200000	0.297E-02	−0.371E-04	0.176E-03	−0.487E-04	0.344E-03	−0.978E-04	0.158E-02
	400000	0.223E-02	−0.460E-04	0.256E-03	−0.774E-04	0.505E-03	−0.156E-03	0.126E-02
	800000	0.174E-02	−0.413E-04	0.313E-03	−0.107E-03	0.623E-03	−0.216E-03	0.109E-02
Si VI 3S-3P	50000	0.842E-02	−0.107E-03	0.361E-04	−0.374E-04	0.690E-04	−0.721E-04	0.436E-02
1314.8 Å	100000	0.598E-02	−0.118E-03	0.927E-04	−0.740E-04	0.179E-03	−0.147E-03	0.309E-02
$C = 0.13$E+21	200000	0.434E-02	−0.116E-03	0.189E-03	−0.129E-03	0.368E-03	−0.260E-03	0.224E-02
	400000	0.326E-02	−0.148E-03	0.295E-03	−0.190E-03	0.582E-03	−0.384E-03	0.180E-02
	800000	0.254E-02	−0.134E-03	0.392E-03	−0.256E-03	0.784E-03	−0.519E-03	0.155E-02
Si VI 3S-3P	50000	0.656E-02	−0.682E-04	0.295E-04	−0.254E-04	0.563E-04	−0.488E-04	0.343E-02
1145.4 Å	100000	0.466E-02	−0.797E-04	0.745E-04	−0.503E-04	0.144E-03	−0.999E-04	0.242E-02
$C = 0.10$E+21	200000	0.338E-02	−0.787E-04	0.149E-03	−0.887E-04	0.290E-03	−0.178E-03	0.175E-02
	400000	0.254E-02	−0.102E-03	0.229E-03	−0.132E-03	0.452E-03	−0.267E-03	0.141E-02
	800000	0.198E-02	−0.909E-04	0.300E-03	−0.179E-03	0.599E-03	−0.364E-03	0.122E-02
Si VI 2P-3S	50000	0.209E-04	−0.851E-06	0.885E-08	0.227E-06	0.169E-07	0.438E-06	0.154E-04
100.2 Å	100000	0.138E-04	0.531E-06	0.665E-07	0.449E-06	0.128E-06	0.891E-06	0.109E-04
$C = 0.73$E+18	200000	0.976E-05	0.815E-06	0.288E-06	0.780E-06	0.571E-06	0.157E-05	0.791E-05
	400000	0.740E-05	0.981E-06	0.709E-06	0.114E-05	0.143E-05	0.231E-05	0.628E-05
	800000	0.577E-05	0.918E-06	0.131E-05	0.153E-05	0.262E-05	0.311E-05	0.541E-05
Si VI 2P-3D	50000	0.267E-04	−0.113E-05	0.147E-06	−0.328E-07	0.280E-06	−0.631E-07	0.194E-04
83.8 Å	100000	0.179E-04	−0.289E-06	0.365E-06	−0.663E-07	0.703E-06	−0.131E-06	0.137E-04
$C = 0.77$E+18	200000	0.130E-04	−0.490E-07	0.715E-06	−0.128E-06	0.139E-05	−0.257E-06	0.969E-05
	400000	0.967E-05	−0.134E-06	0.108E-05	−0.221E-06	0.212E-05	−0.444E-06	0.747E-05
	800000	0.741E-05	−0.802E-07	0.139E-05	−0.321E-06	0.277E-05	−0.647E-06	0.631E-05
Si VI 2P-3D	50000	0.266E-04	−0.116E-05	0.147E-06	−0.165E-07	0.280E-06	−0.318E-07	0.193E-04
83.8 Å	100000	0.174E-04	−0.200E-06	0.364E-06	−0.335E-07	0.701E-06	−0.664E-07	0.137E-04
$C = 0.35$E+18	200000	0.125E-04	0.533E-07	0.712E-06	−0.662E-07	0.139E-05	−0.132E-06	0.967E-05
	400000	0.929E-05	−0.605E-08	0.107E-05	−0.121E-06	0.211E-05	−0.243E-06	0.748E-05
	800000	0.709E-05	0.492E-07	0.139E-05	−0.188E-06	0.275E-05	−0.380E-06	0.631E-05
Si VI 2P-3S′	50000	0.202E-04	−0.613E-06	0.106E-07	0.247E-06	0.202E-07	0.475E-06	0.139E-04
96.7 Å	100000	0.135E-04	0.635E-06	0.787E-07	0.484E-06	0.152E-06	0.961E-06	0.984E-05
$C = 0.45$E+18	200000	0.958E-05	0.879E-06	0.317E-06	0.831E-06	0.629E-06	0.167E-05	0.712E-05
	400000	0.728E-05	0.105E-05	0.752E-06	0.121E-05	0.151E-05	0.244E-05	0.564E-05
	800000	0.570E-05	0.993E-06	0.139E-05	0.158E-05	0.278E-05	0.321E-05	0.486E-05

Table 4 – *continued*

Transition	T (K)	w_e	d_e	w_H^+	d_H^+	w_{He}^+	d_{He}^+	w_{MSE}
Si VI 2P-3D′	50000	0.277E-04	−0.116E-05	0.212E-06	−0.144E-07	0.405E-06	−0.277E-07	0.178E-04
81.2 Å	100000	0.176E-04	−0.202E-06	0.504E-06	−0.291E-07	0.972E-06	−0.578E-07	0.126E-04
$C = 0.58E+18$	200000	0.127E-04	0.363E-07	0.935E-06	−0.577E-07	0.183E-05	−0.115E-06	0.902E-05
	400000	0.937E-05	−0.255E-07	0.136E-05	−0.106E-06	0.268E-05	−0.213E-06	0.710E-05
	800000	0.716E-05	0.289E-07	0.166E-05	−0.166E-06	0.330E-05	−0.336E-06	0.612E-05
Si VI 2P-3D′	50000	0.273E-04	−0.119E-05	0.214E-06	−0.231E-07	0.408E-06	−0.445E-07	0.179E-04
81.2 Å	100000	0.174E-04	−0.260E-06	0.508E-06	−0.468E-07	0.981E-06	−0.928E-07	0.126E-04
$C = 0.59E+18$	200000	0.125E-04	−0.196E-07	0.942E-06	−0.916E-07	0.184E-05	−0.183E-06	0.904E-05
	400000	0.923E-05	−0.845E-07	0.137E-05	−0.161E-06	0.270E-05	−0.324E-06	0.710E-05
	800000	0.704E-05	−0.422E-07	0.167E-05	−0.239E-06	0.332E-05	−0.483E-06	0.610E-05
Si VI 2P-3D′	50000	0.270E-04	−0.107E-05	0.219E-06	−0.148E-07	0.419E-06	−0.285E-07	0.179E-04
81.0 Å	100000	0.175E-04	−0.202E-06	0.520E-06	−0.299E-07	0.100E-05	−0.594E-07	0.127E-04
$C = 0.60E+18$	200000	0.126E-04	0.317E-07	0.960E-06	−0.592E-07	0.187E-05	−0.118E-06	0.905E-05
	400000	0.935E-05	−0.301E-07	0.139E-05	−0.109E-06	0.274E-05	−0.218E-06	0.711E-05
	800000	0.714E-05	0.195E-07	0.169E-05	−0.170E-06	0.336E-05	−0.343E-06	0.609E-05
Si VI 3S′-3P′	50000	0.439E-02	−0.460E-04	0.328E-04	−0.168E-04	0.626E-04	−0.324E-04	0.241E-02
918.8 Å	100000	0.314E-02	−0.597E-04	0.773E-04	−0.333E-04	0.149E-03	−0.662E-04	0.171E-02
$C = 0.40E+20$	200000	0.229E-02	−0.606E-04	0.142E-03	−0.586E-04	0.278E-03	−0.118E-03	0.123E-02
	400000	0.173E-02	−0.737E-04	0.206E-03	−0.869E-04	0.407E-03	−0.176E-03	0.976E-03
	800000	0.135E-02	−0.698E-04	0.252E-03	−0.118E-03	0.500E-03	−0.239E-03	0.845E-03
Si VI 3S-3P	50000	0.510E-02	−0.414E-04	0.244E-04	−0.159E-04	0.465E-04	−0.306E-04	0.263E-02
995.6 Å	100000	0.362E-02	−0.514E-04	0.604E-04	−0.317E-04	0.116E-03	−0.630E-04	0.186E-02
$C = 0.75E+20$	200000	0.263E-02	−0.509E-04	0.118E-03	−0.569E-04	0.230E-03	−0.114E-03	0.134E-02
	400000	0.198E-02	−0.655E-04	0.179E-03	−0.864E-04	0.352E-03	−0.175E-03	0.107E-02
	800000	0.155E-02	−0.589E-04	0.230E-03	−0.118E-03	0.458E-03	−0.240E-03	0.923E-03

When the impact approximation is not valid, the ion broadening contribution may be estimated by using the quasi-static approach (Griem 1974; Sahal-Bréchot 1991; Ben Nessib, Ben Lakhdar & Sahal-Bréchot 1996).

Unfortunately, no experimental data are yet available for the Stark broadening parameters so that the comparison is made only with Dimitrijević's (1993) results obtained using the modified semi-empirical formula (Dimitrijević & Konjević 1980). All our values are greater than Dimitrijević's ones. The ratio w_e/w_{MSE} shows in average an agreement within 56 per cent. Low disagreements are usually found for resonance lines, for example for the spectral line $2p^5\ ^2P^\circ$-$2p^4(^3P)3s\ ^2P$ ($\lambda = 100$, 2 Å) the ratio w_e/w_{MSE} is only 1.06 for $T = 800\,000$ K.

4 STARK BROADENING EFFECT IN WHITE DWARF ATMOSPHERES

White dwarfs are separated in two distinct spectroscopic sequences, the DA and non-DA white dwarfs. The former ones display a pure hydrogen (optical) spectrum. The second, helium-rich sequence comprise DO ($T_{eff} > 45\,000$ K), DB ($11\,000 < T_{eff} < 30\,000$ K) and DC ($T_{eff} < 11\,000$ K) white dwarfs. At the highest effective temperatures the DOs are connected to the helium, carbon and oxygen-rich PG 1159.

Silicon, in various ionization stages, is present in the DO white dwarf atmospheres (Werner et al. 1995). We used our results for Stark widths to examine the importance of electron-impact broadening in atmospheres of DO white dwarfs for a trace element like Si VI. Model atmospheres were taken from Wesemael (1981).

In hot star atmospheres, besides electron-impact broadening (Stark broadening), the important broadening mechanism is a Doppler (thermal) one as well as the broadening due to the turbulence and stellar rotation. Other types of spectral line broadening, such as van der Waals, resonance and natural broadening, are usually negligible. For a Doppler-broadened spectral lines, the intensity distribution is not Lorentzian as for electron-impact broadening but Gaussian, whose full half-width of the spectral lines may be determined by the equation (see e.g. Konjević 1999)

$$w_D\,[\text{Å}] = 7.16 \times 10^{-7} \lambda\,[\text{Å}] \sqrt{\frac{T\,[\text{K}]}{M_{Si}}}, \quad (6)$$

where atomic weight for silicon is $M_{Si} = 28.1$ au.

The importance of Stark broadening in stellar atmospheres is illustrated in Figs 1–4. In Fig. 1 Stark (FWHM) and Doppler widths for Si VI $2p^4(^3P)3s\ ^2P$-$2p^4(^3P)3p\ ^2D^\circ$ ($\lambda = 1226$, 7 Å) spectral line as a function of atmospheric layer temperatures are shown. Stark widths are shown for six atmospheric models with effective temperature $T_{eff} = 50\,000$–$100\,000$ K and logarithm of surface gravity $\log g = 8$. We can see in Fig. 1 that Stark broadening is more important than Doppler broadening for deeper atmospheric layers for all effective temperatures. For white dwarf with effective temperature $T_{eff} = 50\,000$ K, Stark and Doppler widths are equal for temperature layer $T \approx 70\,000$ K, and for white dwarf with effective temperature $T_{eff} = 100\,000$ K, Stark and Doppler are equal for temperature layer $T \approx 125\,000$ K. One should take into account, however, that even when the Doppler width is larger than Stark width, due to different behaviour of Gaussian and Lorentzian distributions, Stark broadening may be important in line wings. In Fig. 2 we present Stark (FWHM) and Doppler widths for Si VI ($\lambda = 1226$, 7 Å) spectral line

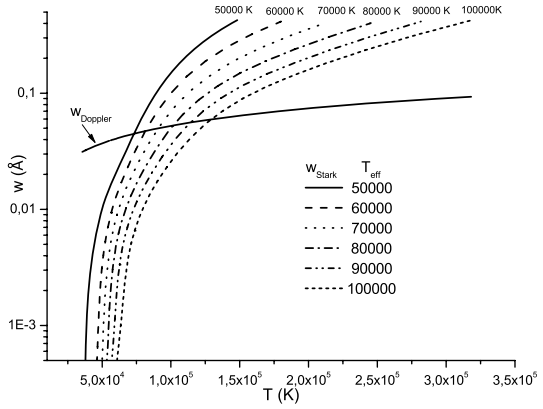

Figure 1. Stark and Doppler widths for Si VI $2p^4(^3P)3s\ ^2P\text{-}2p^4(^3P)3p\ ^2D^\circ$ ($\lambda = 1226,7$ Å) spectral line as a function of atmospheric layer temperatures. Stark widths are shown for six atmospheric models with effective temperature $T_{\rm eff} = 50\,000$–$100\,000$ K and $\log g = 8$.

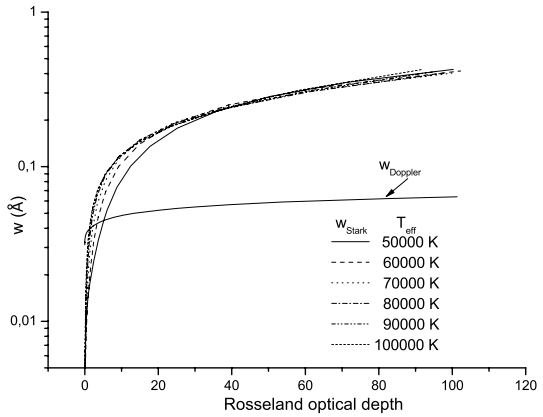

Figure 2. Stark and Doppler widths for Si VI $2p^4(^3P)3s\ ^2P\text{-}2p^4(^3P)3p\ ^2D^\circ$ ($\lambda = 1226,7$ Å) spectral line as a function of Rosseland optical depth. Stark widths are shown for six atmospheric models with effective temperature $T_{\rm eff} = 50\,000$–$100\,000$ K and $\log g = 8$.

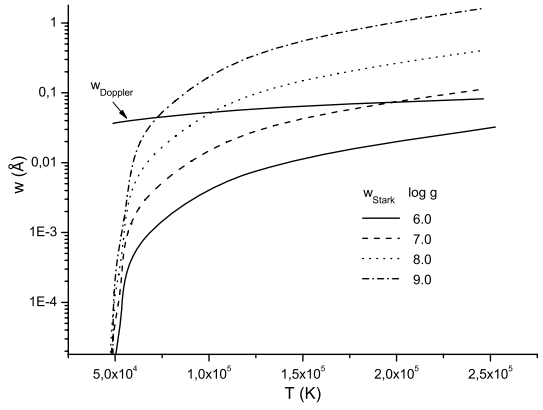

Figure 3. Stark and Doppler widths for Si VI $2p^4(^3P)3s\ ^2P\text{-}2p^4(^3P)3p\ ^2D^\circ$ ($\lambda = 1226,7$ Å) spectral line as a function of atmospheric layer temperatures. Stark widths are shown for four values of model gravity $\log g = 6$–9, $T_{\rm eff} = 80\,000$ K.

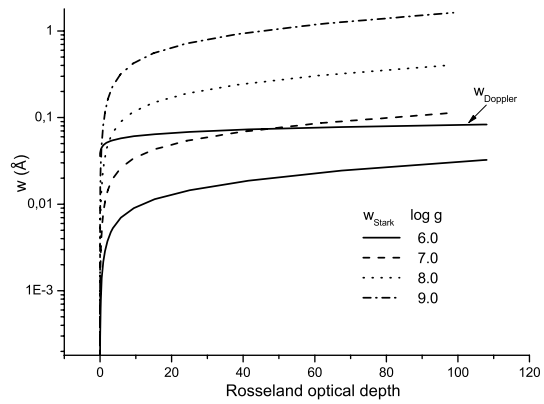

Figure 4. Stark and Doppler widths for Si VI $2p^4(^3P)3s\ ^2P\text{-}2p^4(^3P)3p\ ^2D^\circ$ ($\lambda = 1226,7$ Å) spectral line as a function of Rosseland optical depth. Stark widths are shown for four values of model gravity $\log g = 6$–9, $T_{\rm eff} = 80\,000$ K.

as a function of Rosseland optical depth for the same atmospheric models as in Fig. 1.

The dependence of Stark and Doppler broadening in atmospheric layer temperature for four values of surface gravity is shown in Fig. 3. Atmospheric models used here have effective temperature $T_{\rm eff} = 80\,000$ K. For stellar atmosphere with higher values of surface gravity ($\log g = 8$–9), Stark broadening is significantly larger than Doppler one. For stellar atmosphere with surface gravity $\log g = 7$, Stark widths are comparable to Doppler widths only for deeper hot atmospheric layer. For stellar atmospheres with $\log g = 6$, Doppler broadening is dominant for all atmospheric layers.

5 CONCLUSIONS

In present work we have calculated *ab initio* energy levels for the eight lowest configurations of Si VI. We have also calculated transition probabilities and oscillator strengths for 288 transitions. These data are useful for interpretation of laboratory and astrophysical spectra, since the reliability of the predicted emergent spectra and the derived spectral diagnoses is directly influenced by the quality of radiative data. The method used here is semirelativistic one, the relativistic corrections are included by using the Breit–Pauli Hamiltonian as perturbation to the non-relativistic Hamiltonian. To make fully relativistic calculation, the GRASP code (Dyall et al. 1989) can be used. One should note also that Martin & Wiese (1976) investigated the influence of relativistic effects on the oscillator strength values for the lithium isoelectronic sequences and found that the influence is not important on investigated f values for the ionization degrees investigated in our work. We have reported results of Stark broadening parameter calculations for 15 spectral lines of Si VI. For the simple spectrum, the Stark broadening parameters of different lines are nearly the same within a multiplet (Wiese & Konjević 1992). Consequently, we have used the averaged atomic data for a multiplet as a whole and calculate the corresponding Stark widths and shifts. We see that using the SUPERSTRUCTURE code one obtains a set of energy levels and oscillator strengths, enabling a calculation of Stark broadening parameters when other theoretical and experimental data do not exist. The Stark broadening parameters obtained here, contribute to the creation of a set of such data for as large as possible number of spectral lines, of significance for a number of problems in astrophysical, laboratory and technological plasma research. Our analysis of the influence of Stark broadening on Si VI

($\lambda = 1226,7$ Å) spectral line for stellar plasma conditions demonstrates the importance of this broadening mechanism for hot, high gravity star atmospheres, as for example DO white dwarfs.

ACKNOWLEDGMENTS

We would like to thank C. J. Zeippen for providing his version of SUPERSTRUCTURE code. This work is a part of the projects 146001 'Influence of Collisional Processes on Astrophysical Plasma Line Shapes' and 146002 'Astrophysical Spectroscopy of Extragalactic Objects' supported by the Ministry of Science of Serbia.

REFERENCES

Bates D. R., Damgaard A., 1949, Philos. Trans. R. Soc. Lond. A, 242, 101
Ben Nessib N., Ben Lakhdar Z., Sahal-Bréchot S., 1996, Phys. Scr., 54, 608
Ben Nessib N., Dimitrijević M. S., Sahal-Bréchot S., 2004, A&A, 423, 397
Casassus S., Roche P. F., Barlow M. J., 2000, MNRAS, 314, 657
Coutinho L. H., Trigueiros A. G., 1999, ApJS, 121, 591
Dimitrijević M. S., 1993, A&AS, 100, 237
Dimitrijević M. S., Konjević N., 1980, J. Quant. Spectrosc. Radiat. Transfer, 24, 451
Dimitrijević M. S., Sahal-Bréchot S., 1984, J. Quant. Spectrosc. Radiat. Transfer, 31, 301
Dimitrijević M. S., Sahal-Bréchot S., 1996, Phys. Scr., 54, 50
Dimitrijević M. S., Sahal-Bréchot S., Bommier V., 1991, A&AS, 89, 581
Dimitrijević M. S., Ryabchikova T., Simić Z., Popović L.Č., Dačić M., 2007, A&A, 469, 681
Dyall K. G., Grant I. P., Johnson C. T., Parpia F. A., Plummer E. P., 1989, Comput. Phys. Commun., 55, 424
Eissner W., Jones M., Nussbaumer H., 1974, Comput. Phys. Commun., 8, 270
Fleurier C., Sahal-Bréchot S., Chapelle J., 1977, J. Quant. Spectrosc. Radiat. Transfer, 17, 595
Froese Fischer C., Tachiev G., 2004, At. Data Nucl. Data Tables, 87, 1
Griem H. R., 1974, Spectral Line Broadening by Plasmas. McGraw-Hill, New York
Hamdi R., Ben Nessib N., Dimitrijević M. S., Sahal-Bréchot S., 2007, ApJS, 170, 243
Konjević N., 1999, Phys. Rep., 316, 339
Martin G. A., Wiese W. L., 1976, J. Phys. Chem. Ref. Data, 5, 537
Nussbaumer H., Storey J. P., 1978, A&A, 64, 139
Popović L.Č., Simić S., Milovanović N., Dimitrijević M. S., 2001, ApJS, 135, 109
Sahal-Bréchot S., 1969a, A&A, 1, 91
Sahal-Bréchot S., 1969b, A&A, 2, 322
Sahal-Bréchot S., 1974, A&A, 35, 319
Sahal-Bréchot S., 1991, A&A, 245, 322
Savin D. W., 2001, in Ferland G., Savin D. W., eds, ASP Conf. Ser. Vol. 247, Spectroscopic Challenges of Photoionized Plasmas. Astron. Soc. Pac., San Francisco, p. 167
Uzelac N. I., Glenzer S., Konjević N., Hey J. D., Kunze H. J., 1993, Phys. Rev. E, 47, 3623
Werner K., Dreizler S., Wolff B., 1995, A&A, 298, 567
Wesemael F., 1981, ApJS, 45, 177
Wiese W. L., Konjević N., 1992, J. Quant. Spectrosc. Radiat. Transfer, 47, 185
Zeippen C. J., Seaton M. J., Morton D. C., 1977, MNRAS, 181, 527

This paper has been typeset from a TEX/LATEX file prepared by the author.